Four-dimensional cone-beam computed tomography and digital tomosynthesis reconstructions using respiratory signals extracted from transcutaneously inserted metal markers for liver SBRT[a)]

Justin C. Park
Center for Advanced Radiotherapy Technologies, University of California San Diego, La Jolla, California 92093 and Department of Radiation Oncology, University of California San Diego, La Jolla, California 92093

Sung Ho Park, Jong Hoon Kim,[b),c)] Sang Min Yoon, and Su Ssan Kim
Department of Radiation Oncology, Asan Medical Center, College of Medicine, University of Ulsan, 388-1 Poongnap-Dong, Songpa-gu, Seoul 138-736, South Korea

Jin Sung Kim
Department of Radiation Oncology, Samsung Medical Center, Seoul, South Korea

Zhaowei Liu
Department of Electrical and Computer Engineering, University of California San Diego, La Jolla, California 92093

Tyler Watkins and William Y. Song[b),d)]
Center for Advanced Radiotherapy Technologies, University of California San Diego, La Jolla, California 92093 and Department of Radiation Oncology, University of California San Diego, La Jolla, California 92093

(Received 30 March 2010; revised 20 December 2010; accepted for publication 27 December 2010; published 31 January 2011)

Purpose: Respiration-induced intrafraction target motion is a concern in liver cancer radiotherapy, especially in stereotactic body radiotherapy (SBRT), and therefore, verification of its motion is necessary. An effective means to localize the liver cancer is to insert metal fiducial markers to or near the tumor with simultaneous imaging using cone-beam computed tomography (CBCT). Utilizing the fiducial markers, the authors have demonstrated a method to generate breath-induced motion signal of liver for reconstructing 4D digital tomosynthesis (4DDTS) and 4DCBCT images based on phasewise and/or amplitudewise sorting of projection data.
Methods: The marker extraction algorithm is based on template matching of *a prior* known marker image and has been coded to optimally extract marker positions in CBCT projections from the On-Board Imager (Varian Medical Systems, Palo Alto, CA). To validate the algorithm, multiple projection images of moving thorax phantom and five patient cases were examined. Upon extraction of the motion signals from the markers, 4D image sorting and image reconstructions were subsequently performed. In the case of incomplete signals due to projections with missing markers, the authors have implemented signal profiling to replace the missing portion.
Results: The proposed marker extraction algorithm was shown to be very robust and accurate in the phantom and patient cases examined. The maximum discrepancy of the algorithm predicted marker location versus operator selected location was <1.2 mm, with the overall average of 0.51 ± 0.15 mm, for 500 projections. The resulting 4DDTS and 4DCBCT images showed clear reduction in motion-induced blur of the markers and the anatomy for an effective image guidance. The signal profiling method was useful in replacing missing signals.
Conclusions: The authors have successfully demonstrated that motion tracking of fiducial markers and the subsequent 4D reconstruction of CBCT and DTS are possible. Due to the significant reduction in motion-induced image blur, it is anticipated that such technology will be useful in image-guided liver SBRT treatments.
[DOI: 10.1118/1.3544369]

Key words: marker extraction, motion analysis, 4DCBCT, 4DDTS, liver SBRT

I. INTRODUCTION

The introduction of cone-beam computed tomography (CBCT) system in treatment settings has allowed implementation of various image guidance techniques for precise target localization.[1–5] In particular, the utilization of respiratory correlated four dimensional imaging schemes, such as 4DCBCT[6–11] and 4D digital tomosynthesis (4DDTS),[12,13] for image guidance has been proposed, allowing verification of internal target motion and volume immediately prior to treatment.

Besides the thoracic cancers,[10,11] respiration-induced in-

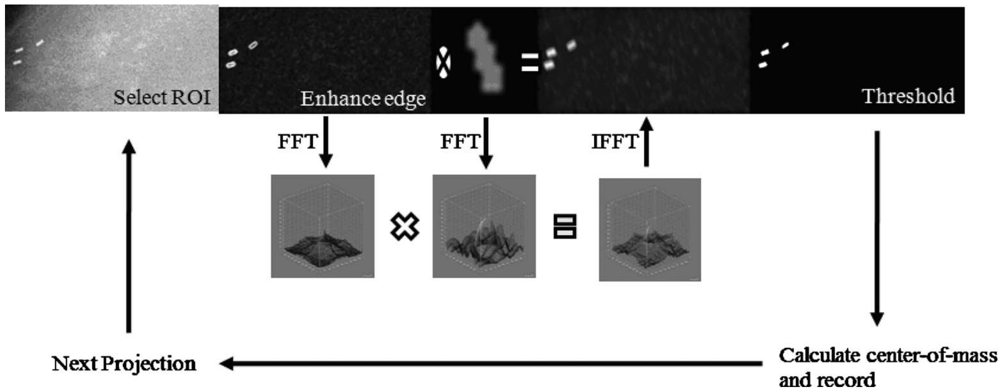

FIG. 1. General workflow of the fiducial marker extraction algorithm.

trafraction tumor motion is also of particular concern in the abdomen such as liver cancer[14,15] necessitating verification prior to treatment. However, unlike lung tumors, the anatomic features of the liver are generally difficult to visualize in CBCT due to the lack of soft tissue contrast,[16] making tumor motion verification challenging. Motivated by this fact, some investigators have inserted metal fiducial markers to or near the tumor to improve image registration accuracy.[17,18] This approach is quite advantageous in that not only the markers can be used for initial image registration but also real-time tumor tracking for treatment is possible.[17]

At present, at least three different approaches have been proposed in acquiring patient breathing signals for 4DCBCT reconstruction; that is, using external sensory systems such as (1) thoracic belt containing a pressure sensor,[19] (2) infrared reflector/marker and/or camera system,[20,21] and using direct approach of (3) detecting anatomical surrogates on the projection data.[6] Methods using external sensory systems can be problematic since it could increase the complexity during patient setup and possible occurrence of correlation-shift between signal and target motion.[22,23] Methods that detect anatomical surrogates such as diaphragms are simple to implement clinically but some can only be used with phasewise sorting.[6]

In this work, we will demonstrate the use of fiducial markers imaged with CBCT projections to generate breath-induced motion signals of liver for 4D image guidance applications. This method is advantageous to the aforementioned techniques since the motion signals are extracted directly from the markers located at or near the tumor, thus giving the most accurate representation of the motion states. In addition, since the marker-derived respiratory signal is used for sorting, 4DCBCT will contain clear marker shapes and locations for guiding accurate image registration for image-guided radiation therapy (IGRT).

II. MATERIALS AND METHODS

II.A. Data acquisition

The projection data were acquired using On-Board Imager (OBI) (Varian Medical Systems, Palo Alto, CA) system, which consists of *a*-Si flat panel detector and kV x-ray source mounted on Varian Trilogy linear accelerator. The flat panel detector consists of 1024×768 pixels with a pixel size of 0.388×0.388 mm. The measured source to imager distance was approximately 150 cm with gantry rotation speed of 6 deg/s (i.e., $\sim$1 min gantry rotation period). Images were acquired using the standard *full-fan* and *half-fan* modes with aluminum full- and half-bow-tie filter, where 360 and 670 2D cone-beam projection data were obtained over 200° and 360° using 100 and 125 kVp, 80 mA, and 25 ms/frame setting, respectively.

II.B. Extraction of fiducial marker positions from cone-beam projection data

For fiducial marker position extraction, we have implemented a novel and fully automated algorithm using *a priori* known marker shape and size, similar to other template matching techniques.[20,24–27] The algorithm consists of five distinct stages, as illustrated in Fig. 1: (1) Subsample a region of interest (ROI) where fiducial markers are contained in the projection image; (2) apply edge enhancement filter (Canny edge operator[28]) to highlight the features of the markers; (3) calculate fast Fourier transform (FFT) of the image, multiply with the corresponding FFT signal of *a priori* obtained fiducial marker image, then perform inverse FFT; (4) apply universal pixel threshold to extract the shape of the markers; and finally (5) calculate the center-of-mass of each fiducial markers.

In the first step, the reason for subsampling ROI for each projection is to maximize calculation efficiency. This ROI size and location can be conveniently determined before the CBCT scan using digitally reconstructed radiograph of the planning CT data. In the second step, the edge enhancement filter is applied to visualize and enhance the features of the markers. This operation uses a filter based on the first derivative of a Gaussian filter kernel to reduce the image noise, followed by calculating the intensity gradient of the image, thereby enhancing marker features without increasing the noise component. In the third step, the convolution of the processed image with an ideal marker image is carried out to further enhance the marker signal in the image. In the fourth

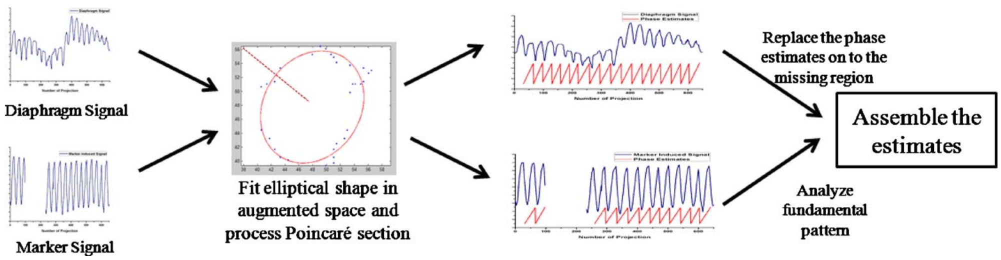

FIG. 2. Signal profiling workflow to estimate motion signals in the missing margin.

and fifth steps, a universal pixel threshold is applied to isolate the markers and to determine their corresponding positions. The algorithm was implemented on MATLAB (The MathWorks Inc., Natick, MA) programming environment. The threshold was set as 80%-value to the maximum pixel value of the processing image.

II.C. Generation of breath-induced marker motion signal

The breath-induced marker motion signal can be generated by compiling the extracted positions of fiducial markers at each cone-beam projection. However, for half-fan scanning geometry, there occasionally exist certain scan angles where fiducial markers are outside of the limited field-of-view (FOV), requiring signal replacement using other references and estimations, the options of which include diaphragm tracking,[6] RPM,[13] and surface markers.[20] Of course, though, it would be ideal to scan in full-fan geometry with markers at or near the center of the projections such that no missing projections would occur.

In this study, we have taken the approach to estimate the marker motion signal in the missing angles through signal *profiling*[29] using the combination of diaphragm motion and prior marker signals. Recently, Ruan *et al.*[29] introduced a real-time approach to systematically estimate baseline, frequency variation, and fundamental pattern change of respiratory signal and subsequently predict the future motion signal based on these prior observations. We have taken a similar approach of motion estimation and this consists of the following three steps as illustrated in Fig. 2: (1) Estimate the phase information through ellipse-fitting in augmented state space and applying Poincaré sectioning principle[29] to the diaphragm signals[6] in the missing angle projections, (2) estimate the most probable amplitude information (i.e., fundamental pattern) through unwarping the prior marker motion signals at each state of phase,[29] and (3) assemble the reconstructed signal estimates.

Note that the purpose of reconstructing signals in the missing projections is to attain complete picture of the breath-induced signal during a patient scan, thereby preserving the overall quality of the 4D reconstructed images. In addition, it is important to recognize that the projections with missing markers will NEVER affect the image quality/integrity of the markers themselves in the reconstructed images since, by definition, these projections do not contain marker information. Therefore, image registration to the markers for patient setup will not be affected negatively in any way.

II.D. Validation of the marker extraction algorithm

For the validation of our proposed marker extraction algorithm (Sec. II B), the following tests were carried out. First, an anthropomorphic thorax phantom with three metal markers embedded was scanned on a programmable motion platform (Fig. 3), with two known input signals: (1) A sine wave with 1.5 cm amplitude and 4 s period and (2) a heavily irregular patient breathing pattern recorded using Respiratory Position Management (RPM) (Varian Medical Systems, Palo Alto, CA) system. The resulting wave forms obtained through the algorithm were compared to the input signals per phase and amplitude. Second, five liver stereotactic body radiotherapy (SBRT) patient cases (with regular and irregular breathing patterns) were used. The reference marker positions were determined manually by an experienced operator checking-off the markers from each projection image on a

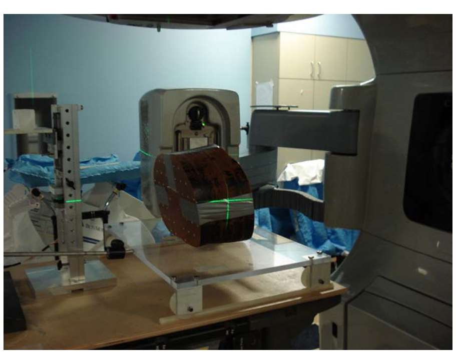

FIG. 3. An anthropomorphic thorax phantom on a programmable motion platform.

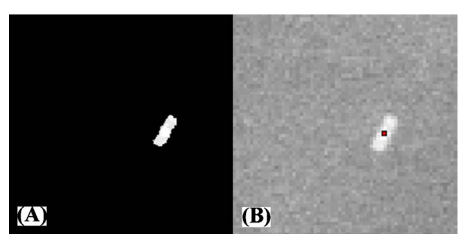

FIG. 4. A typical projection image with marker localization using (a) the marker extraction algorithm and (b) manual check-off.

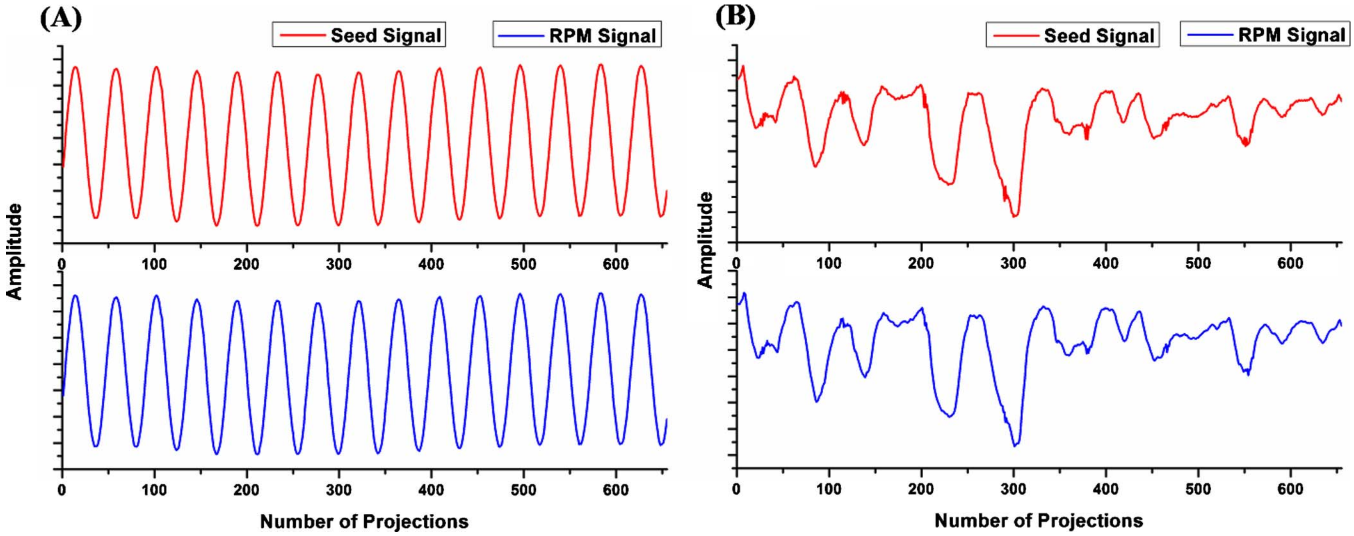

FIG. 5. Comparison of input signal versus extracted signal for (a) a sine wave with 1.5 cm amplitude and 4 s period and (b) an irregular patient breathing pattern.

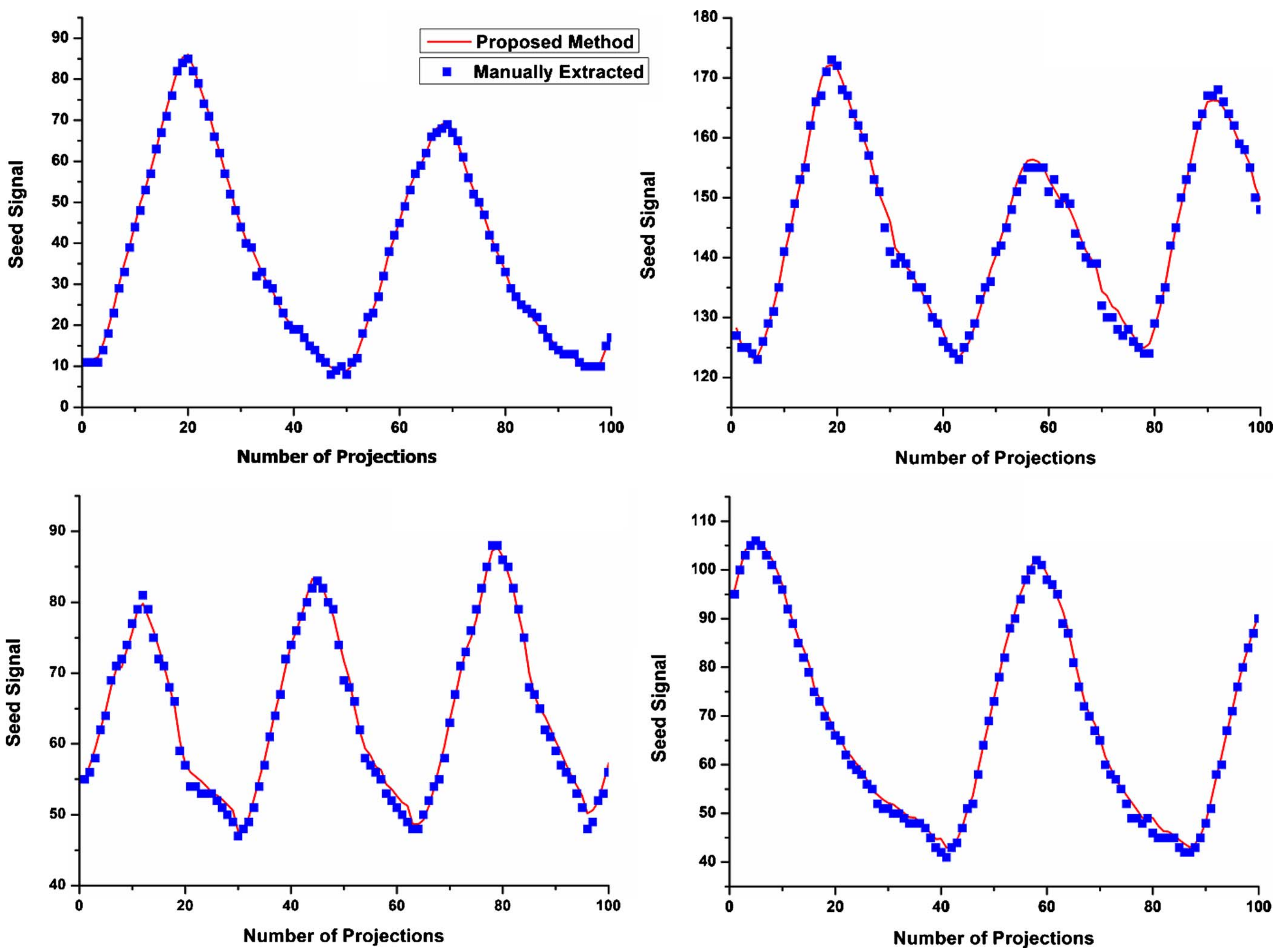

FIG. 6. Overlay of signals extracted using the marker extraction algorithm and the manual check-off for four patient cases.

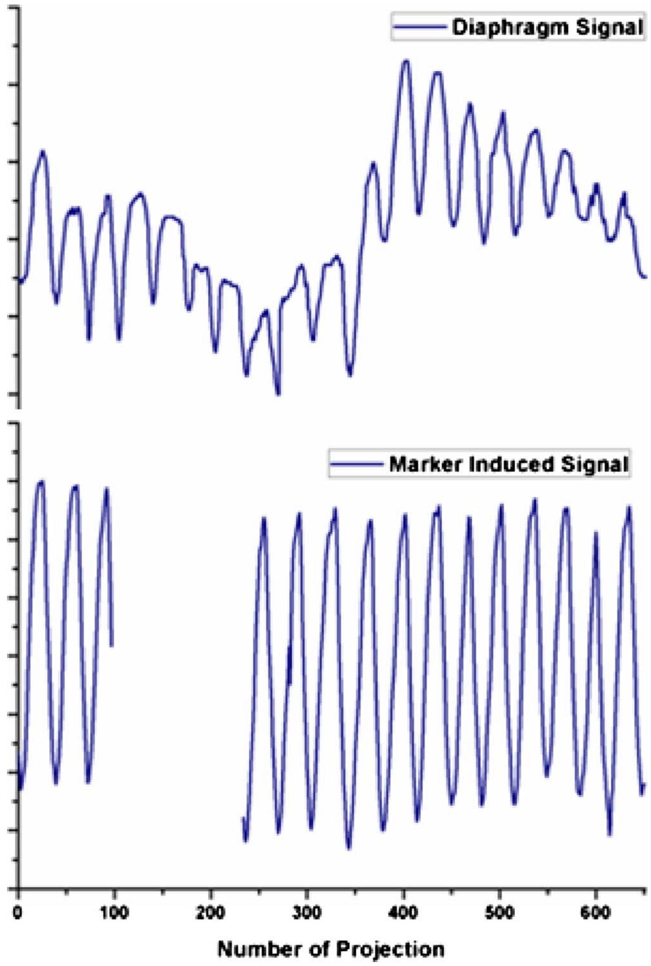

FIG. 7. A typical signal pattern obtained by diaphragm tracking and marker tracking.

computer screen (Fig. 4). This was then compared to the positions determined by the extraction algorithm, for 100 randomly selected projections from each patient, with a total of 500 projections analyzed. Third, for a single patient case, a reference breathing signal was extracted from tracking diaphragm positions in each projection, similar to Sonke *et al.*,[6] and was compared to the signal obtained through the marker tracking algorithm. Finally, metal markers were placed simultaneously on the thorax phantom surface (similar to Li *et al.*[20]) and internally (our work), and both signals were generated using our algorithm to illustrate the differences in the information obtained from placing the markers externally and internally.

II.E. Amplitudewise and phasewise sorting

To illustrate the usefulness of the breathing signals obtained through marker extractions, using the reconstructed motion signals, we have phase- and amplitude-sorted the projections for 4DDTS and 4DCBCT reconstructions. For phase sorting, the projections were divided into four phases; namely, peak-exhale phase, midinhale phase, peak-inhale phase, and midexhale phase. For amplitude sorting, the projections were divided into four amplitudes; namely, low amplitude, midlow amplitude, midhigh amplitude, and high amplitude. The reason for choosing four phases/amplitudes was to balance the image quality with accurate motion representation in the 4D images.

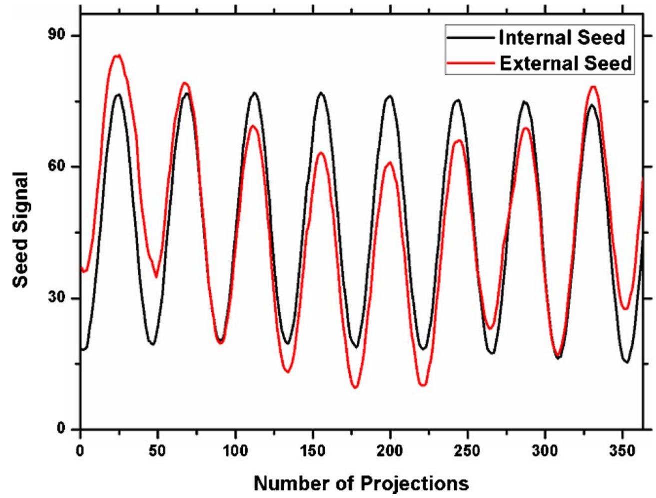

FIG. 8. A typical signal pattern obtained by internal marker tracking and external marker tracking.

In this study, 87.5%–12.5% phases were assigned as peak-exhale, 12.5%–37.5% phases as midinhale, 37.5%–62.5% phases as peak-inhale, and 62.5%–87.5% phases as midexhale phase for phasewise sorting. Similarly, 87.5%–12.5% of signal heights were assigned as low amplitude, 12.5%–37.5% as midlow amplitude, 37.5%–62.5% as midhigh amplitude, and 62.5%–87.5% were assigned as high amplitudes for amplitudewise sorting.

II.F. CBCT and DTS reconstructions

For CBCT reconstruction, the well-known Feldkamp, Davis, and Kress (FDK) algorithm[30] was used. The FDK algorithm was modified to accommodate the half-fan acquisition geometry.[31] The reconstructed volume was set to $512 \times 512 \times 64$ resolution with $1.0 \times 1.0 \times 2.5$ mm pixel dimension in the left-right (LR), anterior-posterior (AP), and superior-inferior (SI) directions, respectively.

For DTS reconstruction, the process is similar to CBCT except that limited angle projections are used.[32,33] Since the current OBI system does not support DTS scan mode, a subset of projections was used for reconstruction, that is, projections from angles $+90° \pm 22.5°$ and $-90° \pm 22.5°$. The reconstructed volume was set to the same resolution as in the CBCT. Both CBCT and DTS reconstruction algorithms were implemented in the C language.

III. RESULTS

Figure 5 shows the comparison between the input signals used to drive the motion platform and the extracted signals obtained from the thorax phantom projections. As can be seen, whether it is regular or irregular patterns, the marker extraction algorithm is robust in reconstructing the true motion signals.

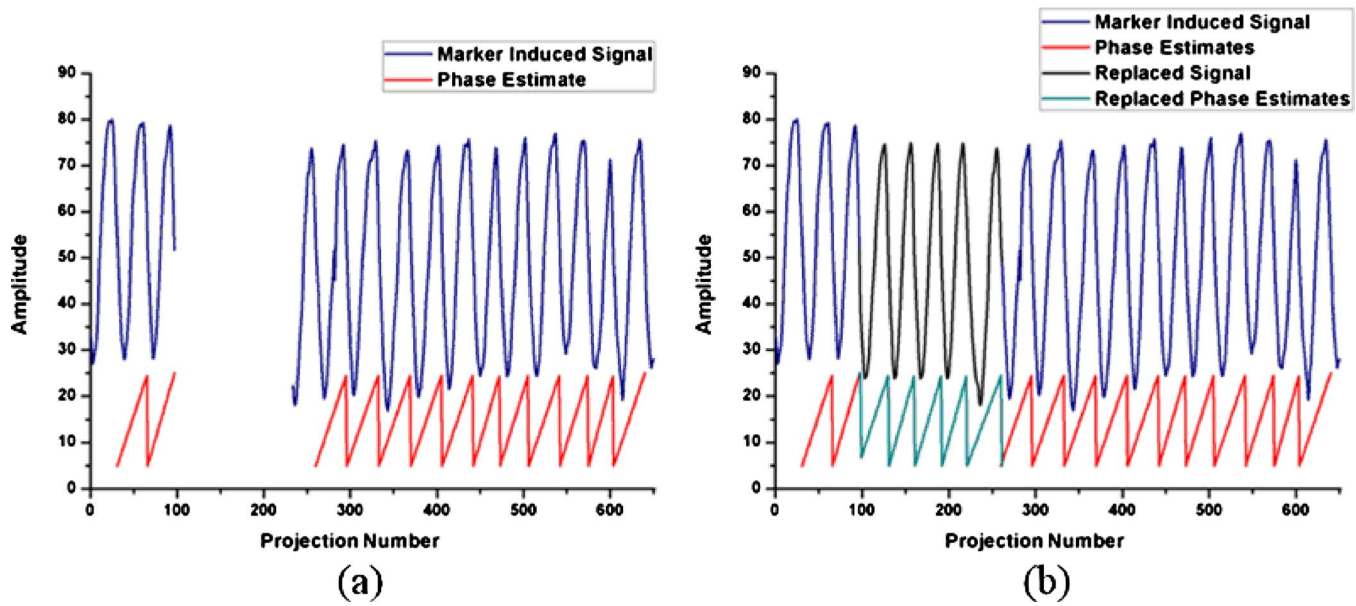

FIG. 9. Marker signal and its corresponding phase/amplitude estimates through signal profiling (a) prior to and (b) after the implementation.

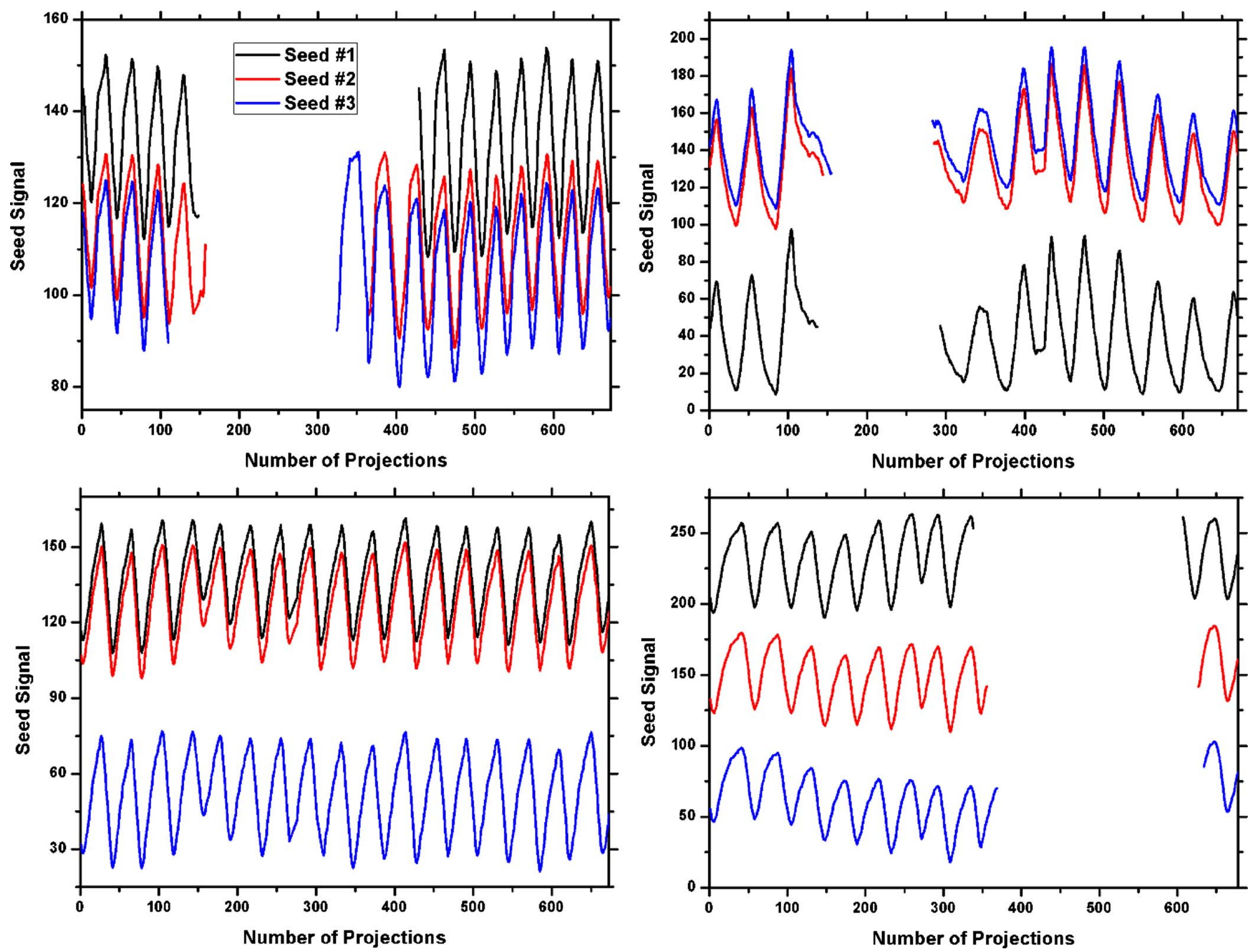

FIG. 10. Marker signals reconstructed for four patient cases.

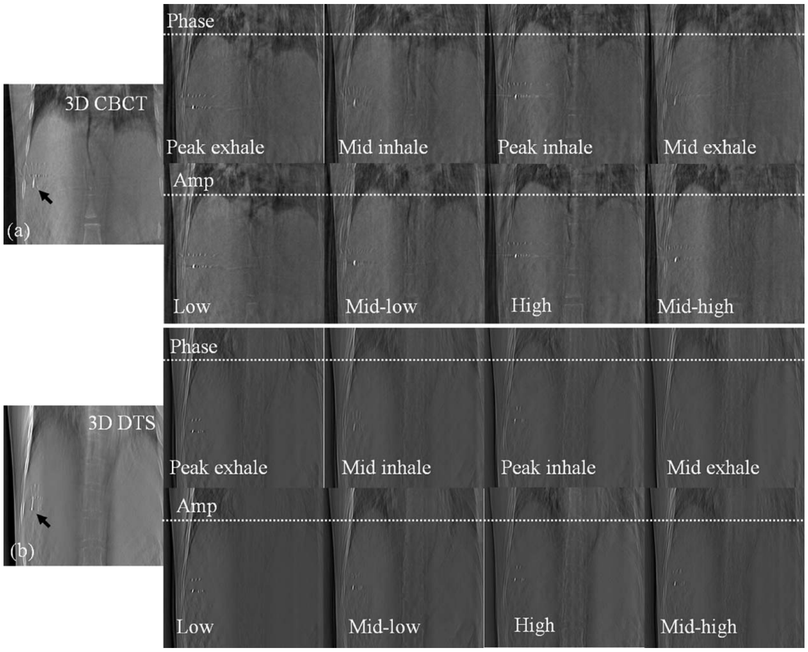

FIG. 11. Phase- and amplitude-sorted (a) 4DCBCT and (b) 4DDTS images with the reference 3D image at the left.

Figure 6 shows the agreement between the operator extracted marker positions and the automated algorithm for four of the five patient cases analyzed. It is to be noted that the spatial resolution of a unit on the Y axis is 0.388 mm. Since no disagreement of more than 3 pixels was observed, the discrepancy between the two methods is <1.2 mm. The overall absolute average discrepancy was 0.51 ± 0.15 mm, however, for the 500 projections analyzed.

Figure 7 illustrates the typical signal patterns that are obtained by diaphragm tracking and internal marker tracking for a sample liver patient. The phases are perfectly synchronized, and hence, both signals are useful. However, as is obvious in the figure, the diaphragm signals can only be used in phase sorting,[6] whereas the marker signals can be used for both phase and amplitude sorting. For marker signals, though, there are missing signal gap (99th–234th projections) due to the half-fan scanning geometry, in this case.

Figure 8 shows the typical signal patterns that are obtained by surface markers and internal markers on the moving thorax phantom. Due to the marker-to-imager magnification effects, the baseline of the surface marker signal drifts sinusoidally, whereas no such effect is observed for the internal marker signal. This suggests that just as diaphragm signals, and unless corrected, surface marker signals can only be used in phase sorting. In addition, for internal markers, the reconstructed images of the markers themselves can be used in image registration for setup guidance, thus, whenever possible, it is more advantageous to place markers near the target volume.

Figure 9 shows the marker motion signal and its corresponding phase and amplitude estimates calculated through signal profiling[29] for the patient in Fig. 7. As can be seen, the replaced signal in the missing region is smooth and without major discontinuities. Remember, though, that if phase sorting is to be performed subsequently with the signals, then the missing signals can be replaced not only through signal profiling but also other methods such as diaphragm tracking, RPM, and surface markers. However, the best approach is to avoid the missing signals altogether by performing full-fan scanning with markers near the center such that the markers are visible in all projections.

Figure 10 shows the marker signals reconstructed for the other four patient cases. As can be seen, the algorithm reliably captures both regular and irregular breathers effectively. For one patient (bottom left), no missing gap occurred as all projections contained the markers.

Figure 11 shows the corresponding phase- and amplitude-sorted reconstruction images of 4DCBCT and 4DDTS using the signal shown in Fig. 9. As can be seen, visually appreciable reduction in motion artifacts (i.e., blurring of markers) are seen in both the phase- and the amplitude-sorted images, in CBCT and DTS. It is anticipated that such marker images

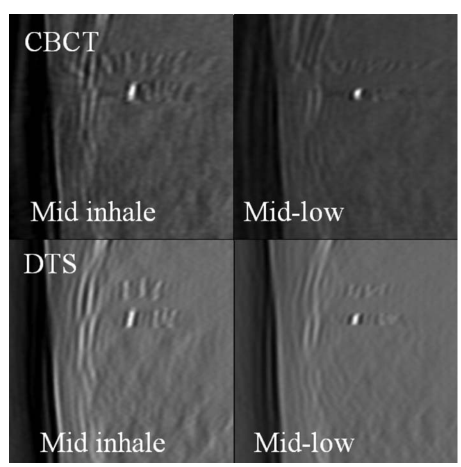

FIG. 12. Magnified view of the midinhale and midlow images in Fig. 11.

would increase the image registration accuracy for liver SBRT setup, the comprehensive evaluation of which is our next work.

To appreciate the fine difference between the phase- and amplitude-sorted images, Fig. 12 shows the magnified view of the midinhale (phase-sorted) and midlow (amplitude-sorted) images containing the markers. As can be seen, the amplitude-sorted midlow images capture the shape of the marker more clearly with less blur. As to how this difference would translate in treatment efficacy is of a future study, however.

IV. DISCUSSION

In this study, we have demonstrated the use of fiducial markers to acquire breath-induced motion signal of liver to generate 4DCBCT and 4DDTS images. To the best of our knowledge, the use of transcutaneously inserted metal markers for 4D image sorting applications in radiation therapy has never been attempted. The proposed method is advantageous in that (1) it does not require external gating system and (2) amplitude- as well as phase sorting is possible, selectively. However, it should be acknowledged that the use of external surrogate-type signals for 4D image sorting applications[9,16,20] is easy and efficient to implement, does not require markers, may be able to do amplitude and phase sorting (e.g., RPM), and should be considered where appropriate along with our proposed approach.

With half-fan geometry, problem arises when fiducial markers are not visualized in the projections due to the limited FOV coverage. However, we have shown that this missing margin can be best replaced/estimated through signal profiling with the diaphragm and prior marker motion signals as the inputs. If in the case the diaphragm is also not visible, then the prior marker motion signal itself can be used so as to predict the approximate phases (e.g., using adaptive learning techniques[29]), as is done with the amplitudes. These predictions may have high uncertainty (e.g., with highly irregular breathing pattern); however, as explained in Sec. II C, such replacement will not be problematic for image guidance applications if only the markers are strictly used for image registration since the fiducial markers are not affected in the reconstructed images. In addition, this problem of missing markers can be completely avoided by using the full-fan scanning geometry, albeit with smaller field of view. However, since only the liver and its immediate surrounding volume really need to be visualized anyway, the full-fan scan usage should be encouraged and recommended. For adaptive replanning and other adaptive radiotherapy applications,[3,10] however, full-fan usage is discouraged, and other approaches should be adapted.[9,16,20]

The results in Fig. 10 have shown that three markers in each patient are generally in high agreement in terms of phase and amplitude. Therefore, using just one of the signals with the most information to reconstruct the images is adequate (which has been done in Fig. 11). However, in the case of marker drift or large organ deformations, causing nonagreement between signals, the best approach may be to average the signals in combination with phase sorting since the phase information will still likely be preserved. Further research, however, is needed to characterize this effect.

Using the homemade software, the marker extraction takes ~0.8 s/projection, subsequent sorting of the images takes ~30 s, and the image reconstruction for a 3DCBCT volume takes ~75 s. This was achieved using a standard PC with Intel® Core2 Quad CPU at 2.66 GHz/processor, 8.0 GB RAM, on a 64-bit operating system. In a busy clinic, these processing times need to be significantly improved to be useful. With the recent interest in graphical processing units (GPU) to accelerate computation times,[33–35] we anticipate that this problem would be easily resolved and is our current work-in-progress.

V. CONCLUSION

In this work, we have successfully demonstrated the feasibility of tumor motion tracking as well as reconstruction of 4DCBCT and 4DDTS images of liver through signal extraction from transcutaneously inserted fiducial markers. It is anticipated that such technology will be useful in image-guided liver SBRT treatments.

ACKNOWLEDGMENTS

W.Y.S. acknowledges that this project is partially supported by the American Cancer Society (ACS) Institutional Research Grant No. 70-002 provided through the Rebecca and John Moores Cancer Center, University of California San Diego. J.S.K. acknowledges that this project is partially supported by the Nuclear Research and Development Program of National Research Foundation of Korea (NRF) Grant No. 2009-0071845 provided by Ministry of Education, Science and Technology (MEST). S.H.P. acknowledges that this research was partially supported by Basic Science Research Program through the National Research Foundation of Korea (NRF) funded by the Ministry of Education, Science and Technology 2010-0012164.

[a]Conflicts of interest: There is no conflict of interest and this is not under consideration for publication elsewhere.

[b]Authors to whom correspondence should be addressed.
[c]Electronic mail: jhkim2@amc.seoul.kr; Telephone: +82- 2-3010-4427; Fax: +82-2-486-7258.
[d]Department of Radiation Oncology, University of California San Diego, Rebecca and John Moores Comprehensive Cancer Center, 3855 Health Sciences Drive #0843, La Jolla, CA 92093-0843; Electronic mail: wysong@ucsd.edu;Telephone: +1-858-246-0886; Fax: +1-858-822-5568.

[1]D. A. Jaffray *et al.*, "Flat-panel cone-beam computed tomography for image-guided radiation therapy," Int. J. Radiat. Oncol., Biol., Phys. **53**(5), 1337–1349 (2002).
[2]D. A. Jaffray, "Emergent technologies for 3-dimensional image-guided radiation delivery," Semin. Radiat. Oncol. **15**(3), 208–216 (2005).
[3]L. Xing *et al.*, "Overview of image-guided radiation therapy," Med. Dosim. **31**(2), 91–112 (2006).
[4]J. P. Bissonnette *et al.*, "Cone-beam computed tomographic image guidance for lung cancer radiation therapy," Int. J. Radiat. Oncol., Biol., Phys. **73**(3), 927–934 (2009).
[5]D. J. Godfrey *et al.*, "Digital tomosynthesis with an on-board kilovoltage imaging device," Int. J. Radiat. Oncol., Biol., Phys. **65**(1), 8–15 (2006).
[6]J. J. Sonke *et al.*, "Respiratory correlated cone-beam CT," Med. Phys. **32**(4), 1176–1186 (2005).

[7]T. Li and L. Xing, "Optimizing 4D cone-beam CT acquisition protocol for external beam radiotherapy," Int. J. Radiat. Oncol., Biol., Phys. **67**(4), 1211–1219 (2007).
[8]T. Li, A. Koong, and L. Xing, "Enhanced 4D cone-beam CT with inter-phase motion model," Med. Phys. **34**(9), 3688–3695 (2007).
[9]J. Lu *et al.*, "Four-dimensional cone beam CT with adaptive gantry rotation and adaptive data sampling," Med. Phys. **34**(9), 3520–3529 (2007).
[10]J. J. Sonke *et al.*, "Frameless stereotactic body radiotherapy for lung cancer using four-dimensional cone beam CT guidance," Int. J. Radiat. Oncol., Biol., Phys. **74**(2), 567–574 (2009).
[11]J. Bissonnette *et al.*, "Quantifying interfraction and intrafraction tumor motion in lung stereotactic body radiotherapy using respiration-correlated cone beam computed tomography," Int. J. Radiat. Oncol., Biol., Phys. **75**(3), 688–695 (2009).
[12]J. Maurer *et al.*, "On-board four-dimensional digital tomosynthesis: First experimental results," Med. Phys. **35**(8), 3574–3583 (2008).
[13]J. Santoro *et al.*, "Evaluation of respiration-correlated digital tomosynthesis in lung," Med. Phys. **37**(3), 1237–1245 (2010).
[14]R. B. Case *et al.*, "Inter- and intrafraction variability in liver position in non-breath hold stereotactic body radiotherapy," Int. J. Radiat. Oncol., Biol., Phys. **75**(1), 302–308 (2009).
[15]M. von Siebenthal *et al.*, "Systematic errors in respiratory gating due to intrafraction deformations of the liver," Med. Phys. **34**(9), 3620–3629 (2007).
[16]A. S. Beddar *et al.*, "4D-CT imaging with synchronized intravenous contrast injection to improve delineation of liver tumors for treatment planning," Radiother. Oncol. **87**(3), 445–448 (2008).
[17]K. Kitamura *et al.*, "Registration accuracy and possible migration of internal fiducial gold marker implanted in prostate and liver treated with real-time tumor-tracking radiation therapy (RTRT)," Radiother. Oncol. **62**(3), 275–281 (2002).
[18]H. Shirato *et al.*, "Feasibility of insertion/implantation of 2.0-mm-diameter gold internal fiducial markers for precise setup and real-time tumor tracking in radiotherapy," Int. J. Radiat. Oncol., Biol., Phys. **56**(1), 240–247 (2003).
[19]L. Dietrich *et al.*, "Linac-integrated 4D cone beam CT: First experimental results," Phys. Med. Biol. **51**(11), 2939–2952 (2006).
[20]T. Li *et al.*, "Four-dimensional cone-beam computed tomography using on-board imager," Med. Phys. **33**(10), 3825–3833 (2006).
[21]S. Leng *et al.*, "High temporal resolution and streak-free four-dimensional cone-beam computed tomography," Phys. Med. Biol. **53**(20), 5653–5673 (2008).
[22]E. Rietzel and G. T. Chen, "Improving retrospective sorting of 4D computed tomography data," Med. Phys. **33**(2), 377–379 (2006).
[23]Y. D. Mutaf, J. A. Antolak, and D. H. Brinkmann, "The impact of temporal inaccuracies on 4DCT image quality," Med. Phys. **34**(5), 1615–1622 (2007).
[24]P. J. Keall *et al.*, "On the use of EPID-based implant marker tracking for 4D radiotherapy," Med. Phys. **31**(12), 3492–3499 (2004).
[25]A. Nederveen *et al.*, "Detection of fiducial gold markers for automatic on-line megavoltage position verification using a marker extraction kernel (MEK)," Int. J. Radiat. Oncol., Biol., Phys. **47**(5), 1435–1442 (2000).
[26]X. Tang, G. C. Sharp, and S. B. Jiang, "Fluoroscopic tracking of multiple implanted fiducial markers using multiple object tracking," Phys. Med. Biol. **52**, 4081–4098 (2007).
[27]R. D. Wiersma, W. Mao, and L. Xing, "Combined kV and MV imaging for real-time tracking of implanted fiducial markers," Med. Phys. **35**(4), 1191–1198 (2008).
[28]J. Canny, "A computational approach to edge detection," IEEE Trans. Pattern Anal. Mach. Intell. **PAMI-8**, 679–698 (1986).
[29]D. Ruan *et al.*, "Real-time profiling of respiratory motion: Baseline drift, frequency variation and fundamental pattern change," Phys. Med. Biol. **54**(15), 4777–4792 (2009).
[30]L. A. Feldkamp, L. C. Davis, and J. W. Kress, "Practical cone beam algorithm," J. Opt. Soc. Am. A **1**(6), 612–619 (1984).
[31]P. S. Cho, R. H. Johnson, and T. W. Griffin, "Cone-beam CT for radiotherapy applications," Phys. Med. Biol. **40**(11), 1863–1883 (1995).
[32]J. T. Dobbins and D. J. Godfrey, "Digital x-ray tomosynthesis: Current state of the art and clinical potential," Phys. Med. Biol. **48**(19), R65–R106 (2003).
[33]J. C. Park *et al.*, "Ultra-fast digital tomosynthesis reconstruction using general-purpose GPU programming for image-guided radiation therapy," Tech. Cancer Res. Treat (submitted).
[34]G. C. Sharp *et al.*, "GPU-based streaming architectures for fast cone-beam CT reconstruction and demons deformable registration," Phys. Med. Biol. **52**(19), 5771–5783 (2007).
[35]H. Yan *et al.*, "Accelerating reconstruction of reference digital tomosynthesis using graphics hardware," Med. Phys. **34**(10), 3768–3776 (2007).